

Article

# Photocatalytic Degradation of Quinoline Yellow over $\text{Ag}_3\text{PO}_4$

Asma Tab <sup>1,2,\*</sup>, Mohamed Dahmane <sup>1</sup> , Belabed Chemseddin <sup>3</sup>, Bachir Bellal <sup>4</sup> ,  
Mohamed Trari <sup>4</sup> and Claire Richard <sup>2,\*</sup> 

<sup>1</sup> Laboratory of Chromatography, Faculty of Chemistry, University of Science and Technology Houari Boumediène, BP 32 El-Alia, Algiers 16111, Algeria; mdahmane.dz@gmail.com

<sup>2</sup> Université Clermont Auvergne, CNRS, SIGMA Clermont, ICCF, F-63000 Clermont-Ferrand, France

<sup>3</sup> Laboratory of Materials Physics, Faculty of Physics, University of Science and Technology Houari Boumediène, BP 32 El-Alia, Algiers 16111, Algeria; bchemsddine@yahoo.fr

<sup>4</sup> Laboratory of Storage and Valorization of Renewable Energies, Faculty of Chemistry, University of Science and Technology Houari Boumediène, BP 32 El-Alia, Algiers 16111, Algeria; bachirbellal60@gmail.com (B.B.); mtrari.usthb@yahoo.fr (M.T.)

\* Correspondence: atab@usthb.dz (A.T.); claire.richard@uca.fr (C.R.); Tel.: +33-(0)4-73-40-7142 (C.R.)

Received: 28 November 2020; Accepted: 9 December 2020; Published: 14 December 2020



**Abstract:** In this study, the ability of  $\text{Ag}_3\text{PO}_4$  to achieve the photocatalytic degradation of quinoline yellow (QY) a hazardous and recalcitrant dye, under UVA and visible light was investigated. The photocatalyst  $\text{Ag}_3\text{PO}_4$  was synthesized through a precipitation method, and characterized by X-ray diffraction (XRD), scanning electron microscope (SEM), BET Brunauer–Emmett–Teller (BET) analysis, UV-Differential Reflectance Spectroscopy (DRS) and Fourier transform infrared spectroscopy (FTIR).  $\text{Ag}_3\text{PO}_4$  could successfully induce the photocatalytic degradation of QY under UVA and visible light. Optimal parameters were  $0.5 \text{ g}\cdot\text{L}^{-1}$  of the catalyst, 20 ppm of QY and  $\text{pH}\sim 7$ .  $\text{Ag}_3\text{PO}_4$  was 1.6-times more efficient than  $\text{TiO}_2$  Degussa P25 under  $\text{UV}_A$  light in degrading QY. Total organic carbon (TOC) analyses confirmed the almost complete QY mineralization. At least eight intermediate degradation products were identified by liquid chromatography coupled to high resolution mass spectrometry. The stability of  $\text{Ag}_3\text{PO}_4$  was satisfactory as less than 5% Ag metal appeared in XRD analyses after 3 reuse cycles. These results show that under optimized conditions  $\text{Ag}_3\text{PO}_4$  can efficiently achieve quinolone yellow mineralization.

**Keywords:**  $\text{Ag}_3\text{PO}_4$ ; visible light; dye; semi-conductor characterization; photoproducts

## 1. Introduction

Advanced Oxidation Processes (AOPs), especially heterogeneous photocatalysis, is an environmentally friendly technique [1] that is used for pollutants elimination in water and air [2], bacterial inactivation [3], reduction of heavy metals to less harmful species and water splitting [4]. Photocatalysis initiates oxidation reactions through the generation of holes ( $\text{h}^+$ ) and electrons ( $\text{e}^-$ ) pairs. The resulting radicals act as oxidants of organic pollutants and convert them into  $\text{CO}_2$ ,  $\text{H}_2\text{O}$ , and inorganic salts [5]. For this reason, extensive investigation was directed toward semiconducting materials that have positive points like the environmental safety and facile preparation. On the other hand, popular photocatalysts such as  $\text{ZnO}$  [6],  $\text{TiO}_2$  [7,8], and  $\text{SnO}_2$  are attractive because of their low cost, environmental friendliness [4], thermal stability and bio safe property [9,10]. However, because they possess a wide gap ( $E_g > 3 \text{ eV}$ ), their efficacy and sensitivity only occur under UV-light making solar-light application not enough efficient [11,12]. In this respect, active research is directed to the elaboration of catalysts active under visible light for the wastewater treatment [13–15].

Recently,  $\text{Ag}_3\text{PO}_4$  has gained great attention as a photocatalyst [16]. It exhibits a high photocatalytic activity upon visible-light irradiation for organic pollutants decomposition [17–20] and selective oxidation of alcohols [18]. Its photocatalytic properties depend on morphology, and active surface area [21–23]. The photocatalytic degradation of anionic dyes by  $\text{Ag}_3\text{PO}_4$  was reported to involve the photogenerated holes that show a high oxidation capability in the valence band [24]. In addition, the existence of  $\text{PO}_4^{3-}$  makes easy the separation of electrons and holes ( $e^-/h^+$ ) pairs through the interfacial junction electric field which generates a dipolar moment.  $\text{Ag}_3\text{PO}_4$  synthesized by a one-step process has shown that both the free radicals and the photo holes generated contribute to the dye mineralization [22]. For application of photocatalysis process in the environmental protection, it is important to use cheap, easily synthesized or readily available photocatalyst.

Dyes are widely used in food and cosmetic products as well as in the textile industries for their variety of colors and their chemical stability. The production of synthetic dyes exceeds 700,000 tons per year, among which 140,000 tons are released in the effluents in a non-controlled way [25]. Given their toxicity [26], these dyes represent an important source of pollution and a serious threat for the aquatic environment [27]. Many dyes show a high stability against temperature, light, and biodegradation [28] making their elimination a major challenge in the water treatment processes. Physico-chemical treatments (coagulation/filtration, coagulation/flocculation, adsorption, etc.) are currently used for the elimination of industrial effluents [29]. However, such techniques do not degrade contaminants but only transfer them from a liquid phase to the solid phase, and additional treatments are thus required [30].

Quinoline Yellow (QY) is a synthetic dye and one of the most employed food additives, even though it has also applications in cosmetic and pharmaceuticals preparations [31]. This dye may cause some diseases like dermatitis and allergic reactions, and has been banned by the standards of the food industry in countries like USA, Australia, Norway, and Iran [32,33]. Many N-containing dyes like QY undergo natural anaerobic reductive degradation, which can generate aromatic amines suspected to be carcinogenic [26]. For these reasons, it is necessary to undertake investigations aiming to eliminate it from water resources. Several studies concerning QY heterogeneous photocatalysis were investigated using ZnO [34],  $\text{TiO}_2$  [34,35] and  $\text{TiO}_2$ /polyaniline composite [36]. However, to our knowledge, product studies are scarce.

Here, we investigated the photocatalytic degradation of QY using  $\text{Ag}_3\text{PO}_4$  as a photocatalyst.  $\text{Ag}_3\text{PO}_4$  was elaborated by a facile method at room temperature, namely the precipitation. The first part of this paper concerns the physical characterization of the material using XRD, SEM, DRS, BET method, and FTIR spectroscopy. It is complementary to the electrochemical properties previously reported [20]. The second part of this paper is focused on the optimization of operating parameters such as pH, catalyst dose and QY initial concentration. Then, photoproducts were characterized by means of ultrafast high-pressure liquid chromatography (UHPLC) coupled to electrospray ionization high-resolution mass spectrometry (ESI-HRMS), while mineralization and the photocatalyst stability were also carried out.

## 2. Results and Discussion

### 2.1. Characterization of $\text{Ag}_3\text{PO}_4$

The XRD pattern of  $\text{Ag}_3\text{PO}_4$  had narrow peaks, characteristic of a high crystallization (Figure 1a). The simulated and the measured diffractograms showed a good fit of 1.6 with  $R_{\text{wp}}$  and  $R_{\text{exp}}$  (%) less than 10% (Figure 1b). The microstructural parameters obtained after the Rietveld refinement were used to determine the dislocation density after elaboration. The coherent domains of diffraction ( $D_v$ ) had an average value of 178 nm and the corresponding microstrain ( $\epsilon$ ) a percentage of  $2.5 \times 10^{-3}$ . It is well known that the presence of crystallographic defects, such as dislocations, has a strong influence on the properties of materials. The dislocation density ( $\rho$ ) calculated from Equations (1)–(3) was  $\rho = 2.6 \times 10^{12}$  in this work. This value is acceptable and confirm the crystal quality. During the elaboration, the dislocation assisted slip activities occurred in the studied material. In addition, the processes used

in this study had no effect on the lattice parameters ( $a = 6.0316$  nm in this work), variation of which is only sensitive to the effects of electronic linkages of the chemical species.

$$\rho = (\rho_D \rho_\epsilon)^{1/2} \quad (1)$$

where  $\rho_D$  and  $\rho_\epsilon$  are calculated using Equations (2) and (3):

$$\rho_D = \frac{3}{Dv^2} \quad (2)$$

$$\rho_\epsilon = \frac{2K\epsilon^2}{b^2} \quad (3)$$

$b$  the Burger vector, and  $K$  is a constant equal to 10 for a Gaussian distribution of the deformations.

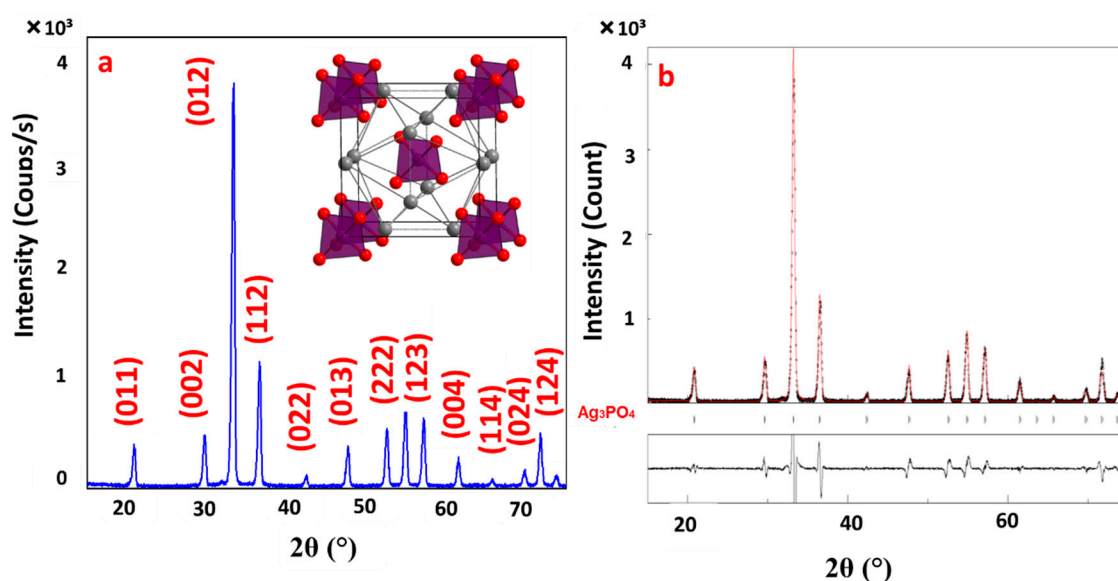


**Figure 1.** XRD spectrum: Identified atomic plane of the  $\text{Ag}_3\text{PO}_4$  phase (a), rietveld refinement of the  $\text{Ag}_3\text{PO}_4$  phase (b).

The SEM micrographs of  $\text{Ag}_3\text{PO}_4$  are illustrated in Figure 2. It can be observed that the morphology of the powder was uniform and agglomerated in spherical grains with regular size lying between 1 and 1.5  $\mu\text{m}$ . The particles surface was relatively smooth. The  $\text{N}_2$  adsorption–desorption isotherm of  $\text{Ag}_3\text{PO}_4$  is shown in Figure 3. The isotherm belonged to the type IV according to IUPAC classification, which indicates a well-developed mesoporous nature. In addition, the desorption isotherm showed a H3-hysteresis, characteristic of a capillary condensation observed in mesoporous structures [36]. The detailed textual parameters of  $\text{Ag}_3\text{PO}_4$  are gathered in Table 1. The specific surface area and total pore volume were equal to  $6 \text{ m}^2 \cdot \text{g}^{-1}$  and  $0.0192 \text{ cm}^3 \cdot \text{g}^{-1}$ , respectively.

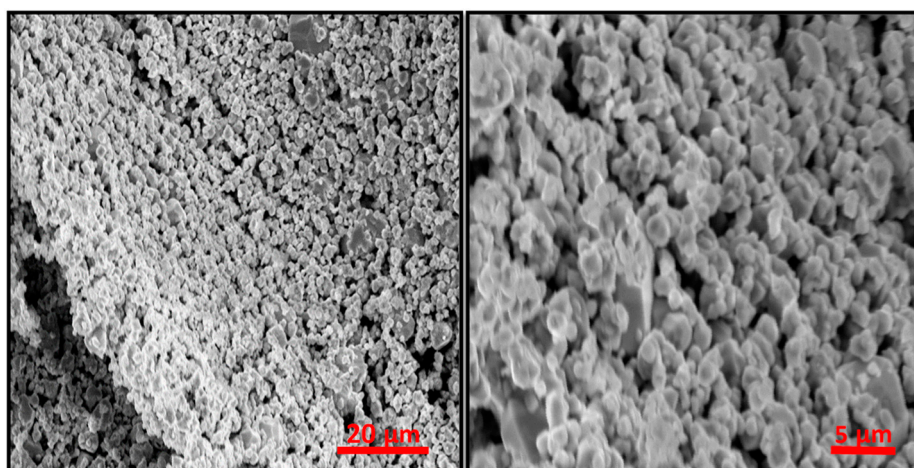


Figure 2. SEM images of  $\text{Ag}_3\text{PO}_4$ .

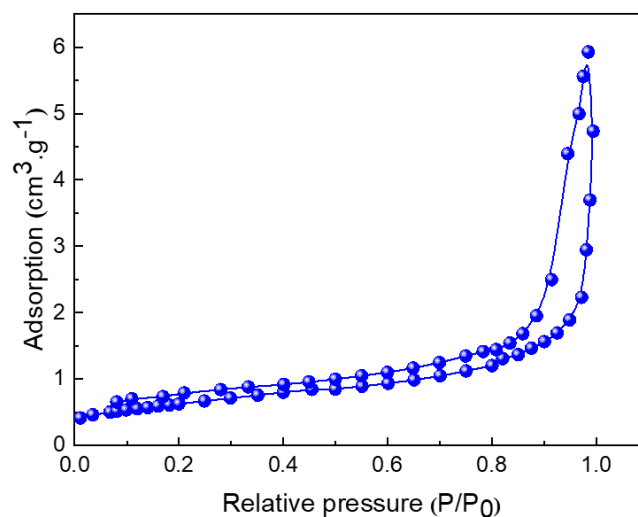


Figure 3. BET of  $\text{Ag}_3\text{PO}_4$  at 77 K.

Table 1. Textural characteristics of  $\text{Ag}_3\text{PO}_4$ .

Sample	Surface Area ( $\text{m}^2\cdot\text{g}^{-1}$ )			Pore Volume ( $\text{cm}^3\cdot\text{g}^{-1}$ )		
	$S_{\text{BET}}$	$S_{\text{ext}}$	$S_{\text{mic}}$	$V_{\text{T}}$	$V_{\text{mes}}$	$M_{\text{mic}}$
$\text{Ag}_3\text{PO}_4$	6	5.18	0.82	0.0192	0.0188	0.0004

The formation of  $\text{Ag}_3\text{PO}_4$  was further supported by the FTIR spectroscopy, using the routine KBr technique in the  $400\text{--}4500\text{ cm}^{-1}$  region. The peaks centered at  $545$  and  $1082\text{ cm}^{-1}$  (Figure 4) were assigned to molecular vibrations of P-O of the phosphate ( $\text{PO}_4^{3-}$ ) unit [18], and the bands at  $3401$  and  $1641\text{ cm}^{-1}$  were attributed to the stretching vibration of O-H groups of adsorbed water. The  $\text{H}_2\text{O}$  molecules and OH groups adsorbed on the surface of  $\text{Ag}_3\text{PO}_4$  are oxidized into free hydroxyl radicals that achieve the photodegradation of organic pollutants [37]. The intense peak at  $1383\text{ cm}^{-1}$  corresponded to the nitrate impurity,  $\text{AgNO}_3$  having been used for the preparation of  $\text{Ag}_3\text{PO}_4$  [38].

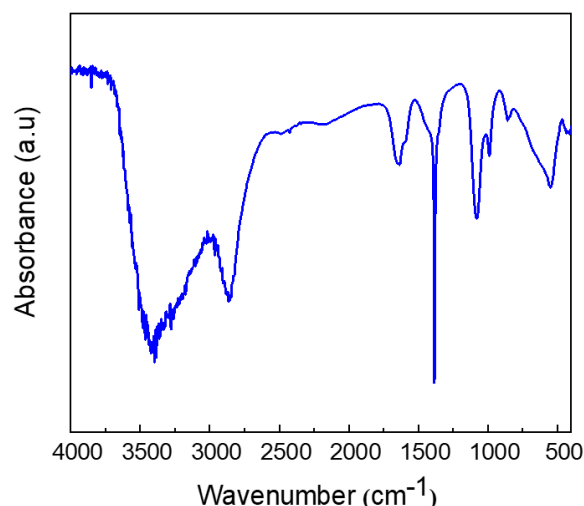


Figure 4. FTIR spectrum of Ag<sub>3</sub>PO<sub>4</sub>.

The knowledge of the gap band ( $E_g$ ) is of great utility in the solar energy conversion; it is evaluated from DRS by using the known relationship:

$$(\alpha_{\lambda} h\nu)^k = \text{Constant} \times (h\nu - E_g) \quad (4)$$

$\alpha_{\lambda}$  ( $\text{cm}^{-1}$ ) is the optical adsorption coefficient and  $h\nu$  (eV) the energy of the incident photon. The nature of the optical allowed transition is deduced from the exponent  $k$  ( $=2$ , direct) or ( $0.5$ , indirect). The gap  $E_g$  is deduced from the intersection of the plot  $(\alpha h\nu)^2$  with the abscissa-axis. The direct transition at 2.52 eV (Figure 5) was in conformity with the yellow color of Ag<sub>3</sub>PO<sub>4</sub> that is a promising photocatalyst under visible light [20].

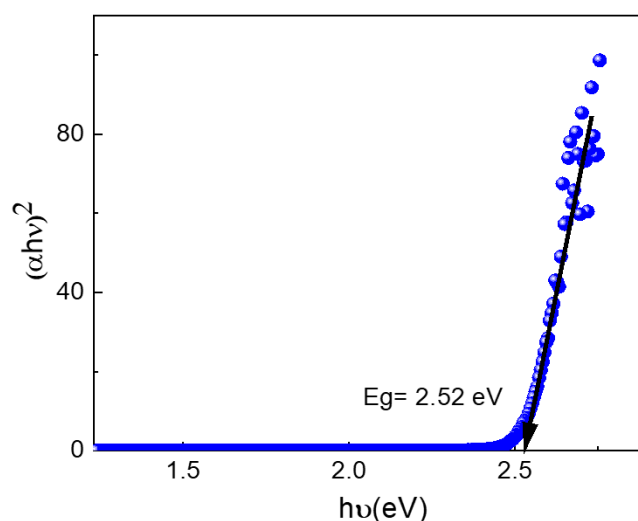
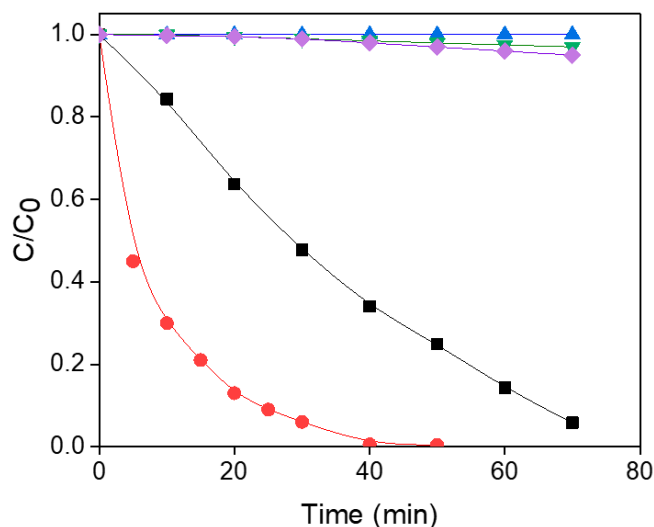


Figure 5. Direct optical transition of Ag<sub>3</sub>PO<sub>4</sub>.

## 2.2. Photocatalytic Degradation of QY

Neither the irradiation of QY under UVA for 4 h in absence of Ag<sub>3</sub>PO<sub>4</sub> nor the stirring of QY solution pH 7 in presence of Ag<sub>3</sub>PO<sub>4</sub> in the dark for 24 h led to a significant concentration loss. These results demonstrated that direct photolysis and adsorption on the photocatalyst were negligible in these conditions. The very poor adsorption of QY on Ag<sub>3</sub>PO<sub>4</sub> in neutral medium can be explained by electrostatic repulsion between the negatively charged surface of the photocatalyst and anionic QY as observed for methyl orange and orange G [39]. In contrast, when the suspension containing

$\text{Ag}_3\text{PO}_4$  and QY was exposed to UVA or visible light, an almost complete degradation was achieved within 40 min and 70 min under visible light and UVA, respectively (Figure 6). Experiments were then undertaken to optimize parameters.



**Figure 6.** Loss of QY (20 ppm) in the absence of  $\text{Ag}_3\text{PO}_4$  under visible light ( $\blacktriangle$ ) or UVA ( $\blacklozenge$ ), in the presence of  $\text{Ag}_3\text{PO}_4$  in the dark ( $\blacktriangledown$ ), upon UVA irradiation ( $\blacksquare$ ) or upon visible light ( $\bullet$ ). ( $[\text{QY}]_0 = 20$  ppm,  $\text{Ag}_3\text{PO}_4$  dose =  $0.5 \text{ g}\cdot\text{L}^{-1}$  and  $\text{pH}\sim 7$ ).

### 2.2.1. Parameters Optimization

In this set of experiments,  $\text{Ag}_3\text{PO}_4$  suspensions were irradiated with visible light. The degradation profile of QY was monitored until 40 min. The QY decrease rate,  $r$ , obeyed an apparent pseudo-first order model ( $r = k \times C$ ); therefore, the degradation rate constants,  $k$ , were obtained from the slope of the plots  $\ln(C/C_0)$  vs. irradiation time.

The photocatalytic degradation of QY (20 ppm) by  $\text{Ag}_3\text{PO}_4$  ( $0.5 \text{ g}\cdot\text{L}^{-1}$ ) was studied by varying pH in the range of 4–11. As shown in Figure 7, the degradation rate of QY was pH-dependent. The highest rate constant ( $0.094 \text{ min}^{-1}$ ) was observed at pH 7. The rate constant drastically decreased below pH 7 by 65–90% while by 40–50% above (Figure 8). This highest efficiency at neutral pH, close to the natural environment, is a very positive point in terms of application.

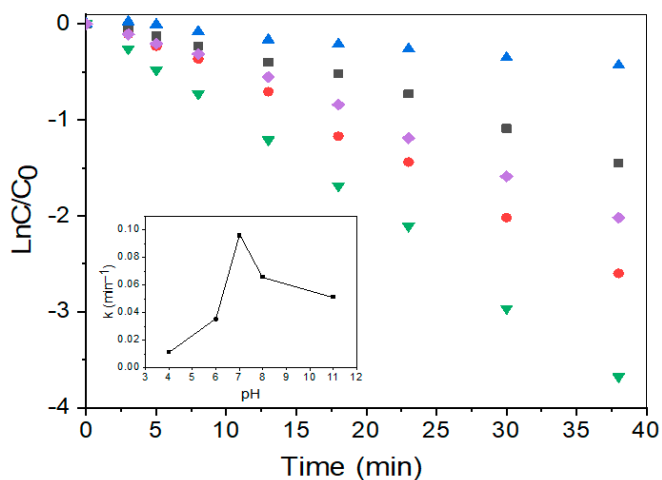


**Figure 7.** Effect of pH on the photocatalytic performance of  $\text{Ag}_3\text{PO}_4$ ,  $\blacktriangle$ : pH = 4,  $\blacksquare$ : pH = 6,  $\blacktriangledown$ : pH = 7,  $\bullet$ : pH = 8,  $\blacklozenge$ : pH = 11. Insert: Rate constants vs. pH ( $[\text{QY}]_0 = 20$  ppm and  $\text{Ag}_3\text{PO}_4$  dose =  $0.5 \text{ g}\cdot\text{L}^{-1}$ ).

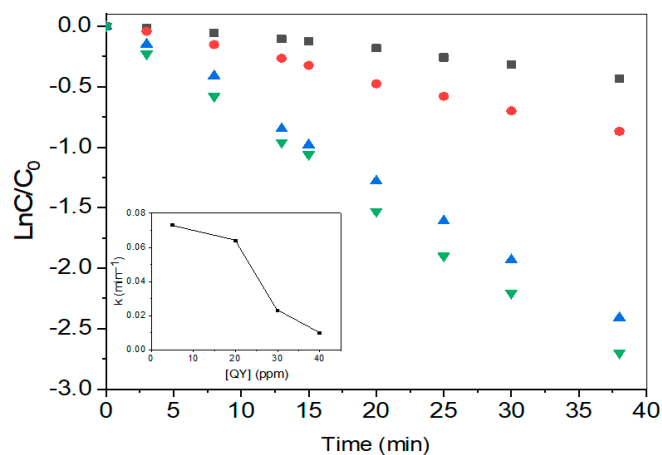


**Figure 8.** Effect of the initial dye concentration  $[QY]_0$  on photocatalytic performance of  $Ag_3PO_4$ ,  $\nabla$ :  $[QY] = 5$  ppm,  $\blacktriangle$ :  $[QY] = 20$  ppm,  $\bullet$ :  $[QY] = 30$  ppm,  $\blacksquare$ :  $[QY] = 40$  ppm. Insert: Rate constants vs.  $[QY]_0$  ( $Ag_3PO_4$  dose =  $0.5\text{ g}\cdot\text{L}^{-1}$  and  $\text{pH}\sim 7$ ).

The reaction was also studied at QY concentrations in the range of 5–40 ppm, at a fixed dose of  $Ag_3PO_4$  ( $0.5\text{ g}\cdot\text{L}^{-1}$ ) and at pH 7. Between 5 and 20 ppm, the rate constant laid between  $0.065$  and  $0.072\text{ min}^{-1}$ , while at 30 and 40 ppm the value dropped to  $0.02$  and  $0.011\text{ min}^{-1}$ , respectively. At 40 ppm, the absorbance of the QY solution was equal to 3.2 at 434 nm, QY had therefore a very strong filter effect and prevents  $Ag_3PO_4$  to absorb light.

The  $Ag_3PO_4$  photocatalyst dose was varied in the range of  $0.25$ – $1\text{ g}\cdot\text{L}^{-1}$  to avoid the photocatalyst excess and ensure a total absorption of efficient incident photons. Figure 9 shows that the degradation rate increased with the catalyst dose and reached a maximum for  $0.5\text{ g}\cdot\text{L}^{-1}$ . The rate constant  $k$  was equal to  $8.6\text{ min}^{-1}$ . An increase in the catalyst dose up to  $1.5\text{ g}\cdot\text{L}^{-1}$  led to a reduced photoactivity due to a lower availability of photoactive sites on the  $Ag_3PO_4$  surface and a weak light utilization [40]. The optimal conditions ( $Ag_3PO_4$  dose =  $0.5\text{ g}\cdot\text{L}^{-1}$ ,  $[QY] = 20$  ppm and  $\text{pH}\sim 7$ ) were kept for experiments under UVA irradiation.

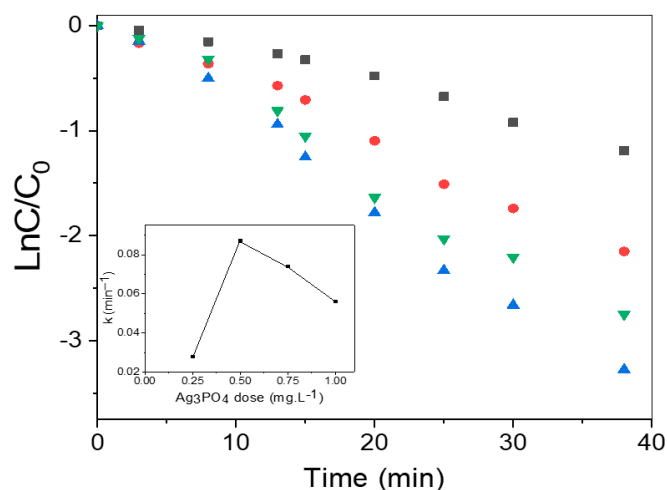


**Figure 9.** Effect of the catalyst dose  $Ag_3PO_4$  on its photocatalytic performance,  $\blacksquare$ :  $0.25\text{ g}\cdot\text{L}^{-1}$ ,  $\blacktriangle$ :  $0.5\text{ g}\cdot\text{L}^{-1}$ ,  $\nabla$ :  $0.75\text{ g}\cdot\text{L}^{-1}$ ,  $\bullet$ :  $1\text{ g}\cdot\text{L}^{-1}$ . Insert: Rate Constants vs.  $Ag_3PO_4$  dose. ( $[QY]_0 = 20$  ppm and  $\text{pH}\sim 7$ ).

## 2.2.2. Compared Photocatalytic Activity $Ag_3PO_4/TiO_2$ Degussa P25

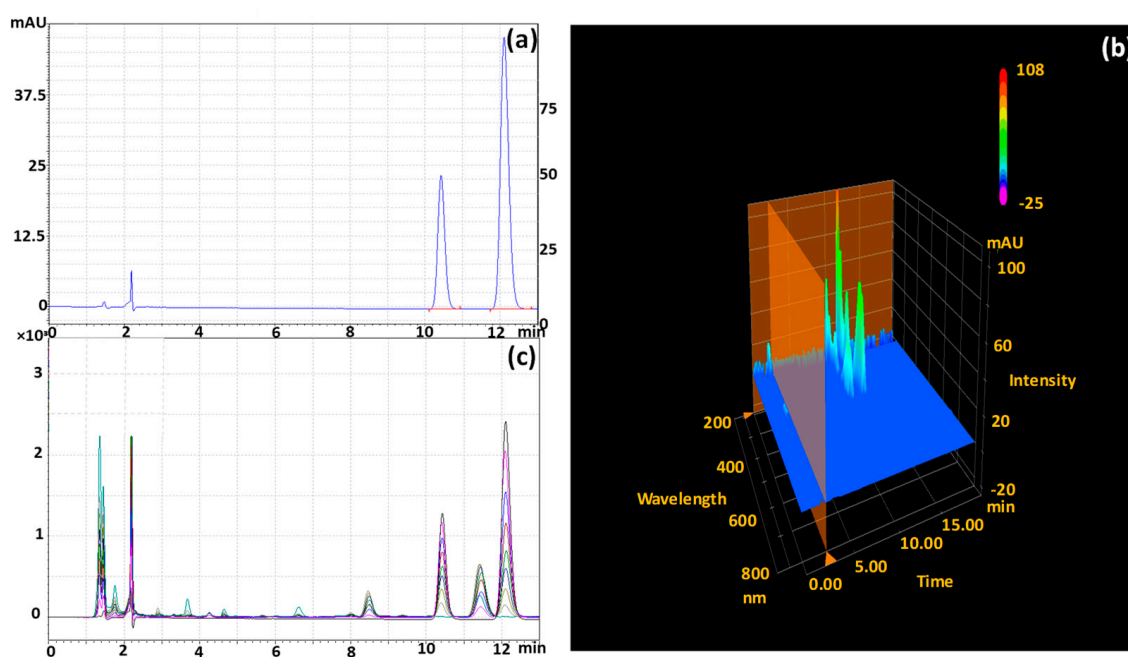
The photocatalytic efficiency  $Ag_3PO_4$  and  $TiO_2$  Degussa P25 (Table 2) were compared at the dose of  $0.5\text{ g}\cdot\text{L}^{-1}$ . Under visible light,  $Ag_3PO_4$  was active while  $TiO_2$  non active and, under UVA,  $Ag_3PO_4$  was 1.6-times more efficient than  $TiO_2$ . This demonstrates the interest of  $Ag_3PO_4$  as a photocatalyst.

**Table 2.** QY degradation rate constants (k) using  $\text{Ag}_3\text{PO}_4$  ( $0.5 \text{ g}\cdot\text{L}^{-1}$ ) or  $\text{TiO}_2$  Degussa P25 ( $0.5 \text{ g}\cdot\text{L}^{-1}$ ) as a photocatalyst.

Conditions	K ( $\text{min}^{-1}$ )	R <sup>2</sup>	Reference
$\text{TiO}_2$ Degussa P25 + QY + UVA	0.018	0.998	This work
$\text{Ag}_3\text{PO}_4$ + QY + UVA	0.029	0.987	This work
$\text{Ag}_3\text{PO}_4$ + QY + Visible light	0.099	0.992	This work
$\text{TiO}_2$ Degussa P25 + QY + Visible light	$<1.8 \times 10^{-4}$		This work

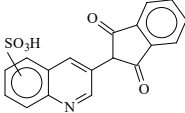
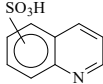
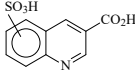
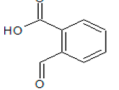
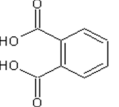
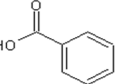
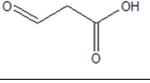
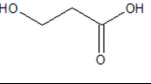
### 2.3. Product Studies

HPLC and UHPLC-ESI-HRMS analyses were conducted for products identification. QY is sold by Sigma-Aldrich as a mixture of mono and disulfonic acids  $\text{C}_{18}\text{H}_{12}\text{NO}_5\text{SNa}$ - $\text{C}_{18}\text{H}_{11}\text{NO}_8\text{S}_2\text{Na}_2$ . Yet, we only detected two peaks at  $m/z = 353.0352$  in  $\text{ES}^-$ . They correspond to two isomeric forms of the monosulfonic acid (Figure 10a,b). Three samples were analyzed after 44, 70 and 175 min of irradiation under UVA. In the first two samples, the QY conversion extent was of 50 and 80%, and in the third one QY was fully degraded (Figure 10c). A typical HPLC chromatogram is shown Figure 10c and Table 3 gives the accurate and experimental  $m/z$ , the chemical formula in the limit of 5 ppm and the possible structure of the 8 detected photoproducts (TPs) by UHPLC-ESI-HRMS. In general, TPs were detected by negative electro spray ionization.



**Figure 10.** 2D HPLC chromatogram (a) and 3D HPLC chromatogram (b): some words have of QY mono-sulfonic acid isomers. HPLC chromatogram of photodegraded QY solution (c). ( $[\text{QY}]_0 = 20 \text{ ppm}$ ,  $\text{Ag}_3\text{PO}_4$  dose =  $0.5 \text{ g}\cdot\text{L}^{-1}$  and  $\text{pH}\sim 7$ ).

Table 3. UHPLC-HRMS data of QY-Ag<sub>3</sub>PO<sub>4</sub> irradiated under UVA.

Compound	Accurate $m/z$ of [M-H] <sup>-</sup>	Exp. $m/z$ of [M-H] <sup>-</sup>	$\Delta$ ppm	Chemical Formula	Proposed Chemical Structure
Quinoline Yellow	353.0352	353.0287	1.84	C <sub>18</sub> H <sub>11</sub> O <sub>5</sub> NS	
TP1	208.0063	208.0074	-2.95	C <sub>9</sub> H <sub>7</sub> O <sub>3</sub> NS	
TP2	251.9961	251.9977	-4.96	C <sub>10</sub> H <sub>7</sub> O <sub>5</sub> NS	
TP3	149.0233	149.0229	2.68	C <sub>8</sub> H <sub>6</sub> O <sub>3</sub>	
TP4	165.0182	165.0187	-3.03	C <sub>8</sub> H <sub>6</sub> O <sub>4</sub>	
TP5	121.0284	121.0286	-1.65	C <sub>7</sub> H <sub>6</sub> O <sub>2</sub>	
TP6	89.0233	89.0231	2.24	C <sub>3</sub> H <sub>6</sub> O <sub>3</sub>	
TP7	87.0077	87.0074	3.45	C <sub>3</sub> H <sub>4</sub> O <sub>3</sub>	
TP8	61.9873	61.9868	-4.6	NO <sub>3</sub> <sup>-</sup>	

TP1 showed  $m/z = 208.0074$  corresponding to C<sub>9</sub>H<sub>7</sub>O<sub>3</sub>NS for the neutral molecule. This TP was likely quinoline sulfonic acid formed by C-C cleavage and its detection allowed us to locate the sulfonic group of QY on the quinoline ring. With  $m/z = 251.9977$ , TP2 had the molecular formula of C<sub>10</sub>H<sub>7</sub>O<sub>5</sub>N and corresponded to TP1 + CO<sub>2</sub>. It was, therefore, likely a carboxylated quinoline sulfonic acid formed by cleavage of the 5-carbon ring. TP3 with  $m/z = 149.0229$  corresponded to a molecular formula of C<sub>8</sub>H<sub>6</sub>O<sub>3</sub>. On the other hand, TP4 that showed  $m/z = 165.018$  corresponded to C<sub>8</sub>H<sub>6</sub>O<sub>4</sub> and most probably to phthalic acid. TP3 might be therefore the corresponding aldehyde. TP5 was identified to benzoic acid ( $m/z = 121.0286$  and C<sub>7</sub>H<sub>6</sub>O<sub>2</sub>). TP6 and TP7 with  $m/z = 89.0231$  and  $87.0074$  were two aliphatic acids with 3 atoms of carbon produced by oxidation and opening of the rings. Nitrate ions ( $m/z = 62.0049$ ) were also detected. TP1–TP5 were detected after 44 and 70 min of irradiation while TP6, TP7 and nitrate ions in the samples irradiated for 175 min. The degradation pathways are summarized in Figure 11.

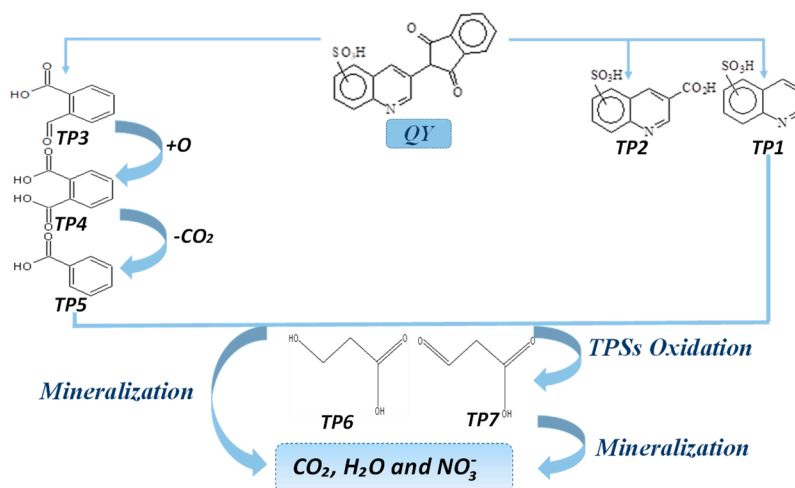


Figure 11. Proposed degradation mechanism for QY in  $\text{Ag}_3\text{PO}_4$  process.

#### 2.4. Mineralization

TOC evolution during the photocatalytic reaction was monitored to explore the percentage of QY mineralization under the optimal conditions (QY 20 ppm,  $\text{Ag}_3\text{PO}_4$  dose =  $0.5 \text{ g}\cdot\text{L}^{-1}$  and pH 7) (Figure 12). After 70 min of irradiation under UVA corresponding to the full degradation of QY, only 5% of OC were transformed into  $\text{CO}_2$ . Total OC removal was reached after 48 h of irradiation time. This long time to achieve complete mineralization indicates that intermediates were difficult to oxidize.

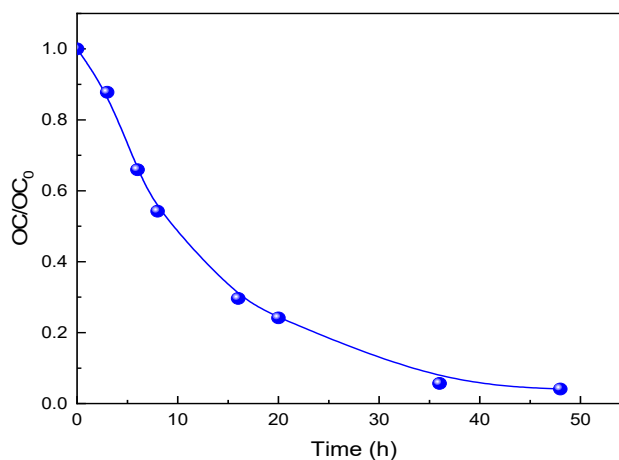
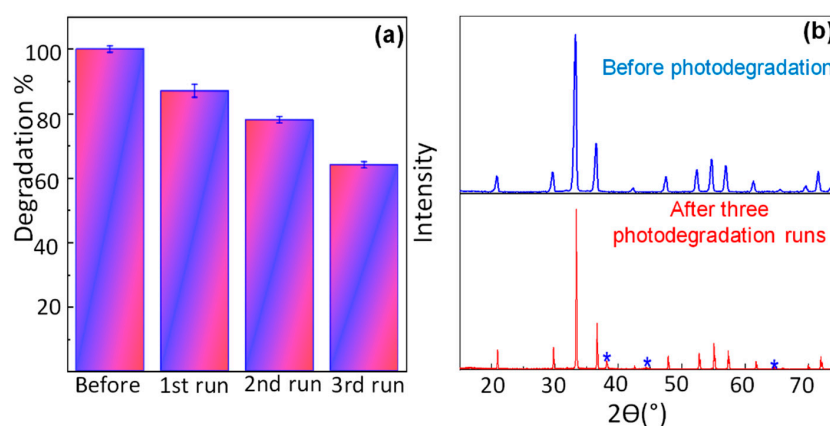


Figure 12. Organic carbon evolution during QY photocatalytic degradation in presence of  $\text{Ag}_3\text{PO}_4$  under UVA.  $[\text{QY}]_0 = 20 \text{ ppm}$ ,  $\text{Ag}_3\text{PO}_4$  dose =  $0.5 \text{ g}\cdot\text{L}^{-1}$  and pH~7).

#### 2.5. Catalyst Stability and Reusability

To assess the photostability and reusability of  $\text{Ag}_3\text{PO}_4$  under visible irradiation for the photodegradation of QY, three photodegradation experiments were successively performed. After each cycle, the catalyst was centrifuged, filtered, thoroughly rinsed with water and ethanol, and finally dried at  $70 \text{ }^\circ\text{C}$ . After three recycles, 87, 78 and 64% of QY were photodegraded (Figure 13a) within 40 min. These results revealed some deactivation effects. This reduction can be explained by the reduction of  $\text{Ag}^+$  to metallic state Ag in the presence of photogenerated electrons. To quantify the percentage of photoreduced  $\text{Ag}^+$ , both XRD and AAS analyses were carried out (Table 4). XRD results after the three cycles are shown in Figure 13b. Small peaks of Ag appeared (<5%) [20]. On the other hand, results of the literature showed that, when dispersed in water and irradiated under visible light for a long time,  $\text{Ag}_3\text{PO}_4$  remained stable (dissolution < 1 ppm) [41]. Atomic absorption spectroscopy analyses confirmed this result (Table 4).



**Figure 13.** Reusability of Ag<sub>3</sub>PO<sub>4</sub> photocatalyst. XRD pattern after three cycles (a). Degradation yield after 40 min of irradiation under visible light for three runs (b). ([QY]<sub>0</sub> = 20 ppm, Ag<sub>3</sub>PO<sub>4</sub> dose = 0.5 g·L<sup>-1</sup> and pH~7).

**Table 4.** Solubility of Ag<sub>3</sub>PO<sub>4</sub> in different conditions.

Conditions	[Ag <sup>+</sup> ] * (ppm)	After 75 min of Irradiation	After 24 h of Irradiation
	Ag <sub>3</sub> PO <sub>4</sub> in the dark		0.018
Ag <sub>3</sub> PO <sub>4</sub> + Visible light		0.017	0.017
Ag <sub>3</sub> PO <sub>4</sub> + QY + Visible light		0.02	0.02

### 3. Experimental

#### 3.1. Chemicals

Quinoline Yellow was a mixture of the mono- and disulfonic acids (acid yellow 3, Sigma-Aldrich, St. Louis, MO, USA, Figure 14). The other chemicals were: titanium dioxide Degussa P25 (TiO<sub>2</sub> P25, 99.5%, Evonik, Essen, Germany), disodium phosphate (Na<sub>2</sub>HPO<sub>4</sub>, 99%, Merck, Kenilworth, NJ, USA), silver nitrate (AgNO<sub>3</sub>, 99.9%, Alfa Aesar, Haverhill, MA, USA), sodium hydroxide (NaOH, 99.99%, Sigma-Aldrich, St. Louis, MO, USA), perchloric acid (HClO<sub>4</sub>, 99.99%, Sigma-Aldrich, St. Louis, MO, USA), sodium acetate for HPLC LiChropur (C<sub>2</sub>H<sub>3</sub>NaO<sub>2</sub>, ≥99%, Supelco, Bellefonte, PA, USA), potassium bromide FT-IR grade (KBr, 99%, Merck, Kenilworth, NJ, USA), formic acid for LC-MS LiChropur (CO<sub>2</sub>H<sub>2</sub>, 98–100%, Supelco, Bellefonte, PA, USA), acetonitrile LiChrosolv hyper grade for LC-MS (CH<sub>3</sub>CN, Merck, Kenilworth, NJ, USA) and acetonitrile gradient grade for HPLC ACS (≥99.9%, Carlo Erba, Cornaredo, Italy). All reagents were used without any purification process. Water was purified using a RIOS 5 reverse osmosis and synergy (Millipore, Burlington, MA, USA) device (resistivity 18 MΩ·cm, DOC < 0.1 mg·L<sup>-1</sup>).

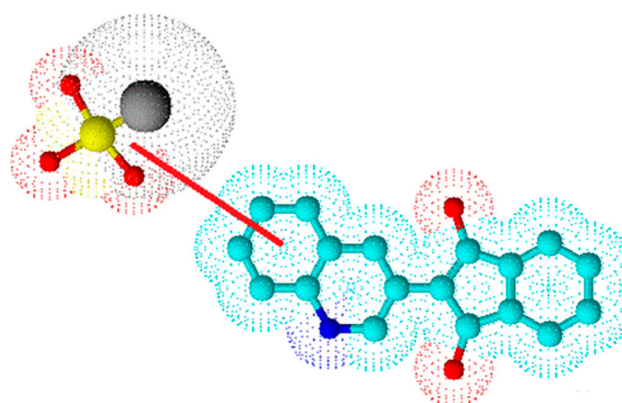


**Figure 14.** Quinoline Yellow structure using ChemSketch software.

### 3.2. Synthesis of $\text{Ag}_3\text{PO}_4$

$\text{Ag}_3\text{PO}_4$  was prepared by precipitation as previously described [20]. Briefly, 15 mL of a  $\text{Na}_2\text{HPO}_4$  solution (3 mM) was mixed dropwise with 30 mL of  $\text{AgNO}_3$  solution (3 mM) under magnetic stirring during 3 h at room temperature. The precipitate with a yellow color characteristic of  $\text{Ag}_3\text{PO}_4$ , was collected and washed with deionized water and ethanol. The yellow powder was recovered after drying at 70 °C under static vacuum overnight.

### 3.3. Characterization of $\text{Ag}_3\text{PO}_4$

The synthesized phase was confirmed by X-ray diffraction using  $\text{Co K}\alpha$  line ( $\lambda = 1.790300 \text{ \AA}$ ) at a  $2\theta$  scan rate of 2 per min. The micrograph of the sample was examined by SEM analysis using a JEOL microscope (Model JSM 6360-LV). The BET surface area and pore volume were calculated from the  $\text{N}_2$  adsorption/desorption isotherm at 77 K using an ASAP 2010 Micrometrics equipment. The external surface area, micropore area and micropore volume were computed by the t-plot technique. The total pore volume was determined from the liquid  $\text{N}_2$  volume at high relative pressure (0.99). The subtraction of the micropore volume from the total volume gave the volume of mesopore. The DRS was measured using a spectrophotometer (Specord 200 Plus). The concentration of Ag before and after recycling in hydrolyzed samples was determined using Atomic Absorption Spectrophotometry (AAS) (Perkin-Elmer A700). A calibration curve was created by analyzing Ag (1, 2, 3, 4  $\mu\text{g}\cdot\text{mL}^{-1}$ ) standard solutions, and the instrument was adjusted to 328.1 nm.

### 3.4. Photocatalytic Experiments

Irradiations were conducted in two devices; one was equipped with fluorescent tubes (Philips HPK 15 W) emitting in the near UV region (maximum at 365 nm) while the other with LED (Delleled 5 W) emitting within the wavelength range 400–800 nm. Pyrex reactors were connected to a thermostatically controlled water bath. For irradiation under visible 50 mL of suspensions containing  $\text{Ag}_3\text{PO}_4$  and QY were added to the reactor of 100 mL of capacity while for UVA irradiation 15 mL of suspensions were placed in the reactor of 30 mL capacity. Solution pH was adjusted using NaOH or  $\text{HClO}_4$ . In both systems, the suspensions were kept at 25 °C under constant agitation (600 rpm). Aliquots of 0.5 mL were regularly withdrawn, vigorously centrifuged and filtered through a 0.45  $\mu\text{m}$  filter (Waters, Millipore) before analyses. The degradation yield (%) was evaluated from the relationship:

$$\text{Degradation in \%} = \frac{C_0 - C_t}{C_0} \times 100 \quad (5)$$

$C_0$  being the initial QY concentration and  $C_t$  the concentration at time (t).

### 3.5. Analytical Analyses

A UV-vis spectrophotometer (Model Specord 200 plus) was used to monitor the degradation of QY ( $\lambda_{\text{max}} = 434 \text{ nm}$ ). QY and its photoproducts were separated using a Shimadzu 8040 HPLC system, equipped with a SPD-M30A DAD detector, and a Nucleodur 100-3  $\text{C}_{18}$  end-capped column (125 mm  $\times$  4.0 mm, 3  $\mu\text{m}$  particle size). The mobile phase was a mixture of (A) 30  $\text{mmol}\cdot\text{L}^{-1}$  sodium acetate and (B) acetonitrile in the proportions of 80% A and 20% B, at a constant flow rate of 0.75  $\text{mL}\cdot\text{min}^{-1}$ . The detection wavelength was set at 290 nm and the temperature oven at 30 °C.

UHPLC-ESI-HRMS was performed on an Orbitrap Q-Exactive (Thermo Scientific, Waltham, MA, USA) mass spectrometer coupled to an Ultimate 3000 RSLC (Thermo Scientific, Waltham, MA, USA) apparatus. The mass spectrometer with heated electrospray ionization was operated in both positive and negative ESI modes with a spray voltage of 3 kV for both modes. The column was a Waters analytical column (2.1  $\times$  100 mm, 1.7  $\mu\text{m}$  particle size) and the column oven temperature was regulated at 30 °C. The aqueous solvent (A) was a mixture of formic acid (0.1%) and acetonitrile as organic phase (B). The separation was

achieved using a gradient program consisting of 0–7.5 min 5%, 7.5–8.5 min 99% of the mobile phase B. The injection volume was taken at 10  $\mu\text{L}$  while the flow rate was fixed at 0.450  $\text{mL}\cdot\text{min}^{-1}$ .

A Shimadzu 5050 TOC analyzer was used to monitor the mineralization of QY. The percentage of mineralization was calculated using the following equation:

$$\text{Mineralization} = \frac{(\text{OC}_0 - \text{OC}_t)}{\text{OC}_0} \times 100 \quad (6)$$

where  $\text{OC}_0$  is the organic carbon present in the solution at time 0 and  $\text{OC}_t$  at time t. OC is obtained by subtracting the inorganic carbon from total carbon.

#### 4. Conclusions

$\text{Ag}_3\text{PO}_4$  was synthesized by precipitation at ambient temperature. It was shown to induce the photocatalytic oxidation of Quinoline Yellow under visible irradiation with an efficiency much higher than that of  $\text{TiO}_2$  Degussa P25 under UVA. The optimal parameters such as initial pH, QY concentration and catalyst dose were determined. Photoproducts of QY were identified based on the UHPLC-ESI-HRMS analysis and were different than those identified using  $\text{TiO}_2$ . The complete mineralization of QY was achieved after 48 h of irradiation against 70 min for QY elimination. Some XRD peaks of Ag metal (~5%) were noticeable after three reuses. It can be concluded that  $\text{Ag}_3\text{PO}_4$  needs efficient hetero-junction to avoid its photocorrosion. This is the subject of our future investigations.

**Author Contributions:** All authors listed have made a substantial, direct and intellectual contribution to the work, and approved it for publication: A.T. methodology and designed the experiments, prepared and wrote the original draft; M.D., B.C., B.B. methodology and designed the experiments, analyzed the experimental data, characterized the material; C.R. methodology and designed the experiments, involved in review and final editing; M.T. conceptualization, funding acquisition, methodology and designed the experiments. All authors have read and agreed to the published version of the manuscript.

**Funding:** This work was supported by the Franco-Algérien “PROFAS B+” program.

**Acknowledgments:** A.T. thanks this program for having granted her stay in the ICCF. The authors thank Martin Lereboure (Engineer CNRS) and Frédéric Emmenegger (Tech CNRS) for the UHPLC-HRMS analyses and Guillaume Vyard (Engineer CNRS) for assistance in chromatographic analyses.

**Conflicts of Interest:** The authors declare no conflict of interest.

#### References

1. Yang, Y.; Li, X.; Zhou, C.; Xiong, W.; Zeng, G.; Huang, D.; Zhang, C.; Wang, W.; Song, B.; Tang, X.; et al. Recent advances in application of graphitic carbon nitride-based catalysts for degrading organic contaminants in water through advanced oxidation processes beyond photocatalysis: A critical review. *Water Res.* **2020**, *184*, 116200. [[CrossRef](#)] [[PubMed](#)]
2. Karpuraranjith, M.; Chen, Y.; Wang, X.; Yu, B.; Rajaboopathi, S.; Yang, D. Hexagonal SnSe nanoplate supported  $\text{SnO}_2$ -CNTs nanoarchitecture for enhanced photocatalytic degradation under visible light driven. *Appl. Surf. Sci.* **2020**, *507*, 145026. [[CrossRef](#)]
3. Yu, H.; Wang, D.; Zhao, B.; Lu, Y.; Wang, X.; Zhu, S.; Qin, W.; Huo, M. Enhanced photocatalytic degradation of tetracycline under visible light by using a ternary photocatalyst of  $\text{Ag}_3\text{PO}_4/\text{AgBr}/g\text{-C}_3\text{N}_4$  with dual Z-scheme heterojunction. *Sep. Purif. Technol.* **2020**, *237*, 116365. [[CrossRef](#)]
4. Wang, J.; Yue, X.; Yang, Y.; Sirisomboonchai, S.; Wang, P.; Ma, X.; Abudula, A.; Guan, G. Earth-abundant transition-metal-based bifunctional catalysts for overall electrochemical water splitting: A review. *J. Alloys Compd.* **2020**, *819*, 153346. [[CrossRef](#)]
5. Mudhoo, A.; Paliya, S.; Goswami, P.; Singh, M.; Lofrano, G.; Carotenuto, M.; Carraturo, F.; Libralato, G.; Guida, M.; Usman, M.; et al. *Fabrication, Functionalization and Performance of Doped Photocatalysts for Dye Degradation and Mineralization: A Review*; Springer International Publishing: Berlin/Heidelberg, Germany, 2020; Volume 18, ISBN 1031102001045.
6. Ong, C.B.; Ng, L.Y.; Mohammad, A.W. A review of ZnO nanoparticles as solar photocatalysts: Synthesis, mechanisms and applications. *Renew. Sustain. Energy Rev.* **2018**, *81*, 536–551. [[CrossRef](#)]

7. Guo, Q.; Zhou, C.; Ma, Z.; Yang, X. Fundamentals of TiO<sub>2</sub> Photocatalysis: Concepts, Mechanisms, and Challenges. *Adv. Mater.* **2019**, *31*, 1901997. [[CrossRef](#)]
8. Vernardou, D.; Stratakis, E.; Kenanakis, G.; Yates, H.M.; Couris, S.; Pemble, M.E.; Koudoumas, E.; Katsarakis, N. One pot direct hydrothermal growth of photoactive TiO<sub>2</sub> films on glass. *J. Photochem. Photobiol. A Chem.* **2009**, *202*, 81–85. [[CrossRef](#)]
9. Chantana, J.; Kawano, Y.; Nishimura, T.; Mavlonov, A.; Minemoto, T. Impact of Urbach energy on open-circuit voltage deficit of thin-film solar cells. *Sol. Energy Mater. Sol. Cells* **2020**, *210*, 110502. [[CrossRef](#)]
10. Fatimah, I.; Nurillahi, R.; Sahroni, I.; Muraza, O. TiO<sub>2</sub>-pillared saponite and photosensitization using a ruthenium complex for photocatalytic enhancement of the photodegradation of bromophenol blue. *Appl. Clay Sci.* **2019**, *183*, 105302. [[CrossRef](#)]
11. Chen, D.; Huang, S.; Huang, R.; Zhang, Q.; Le, T.T.; Cheng, E.; Hu, Z.; Chen, Z. Convenient fabrication of Ni-doped SnO<sub>2</sub> quantum dots with improved photodegradation performance for Rhodamine B. *J. Alloys Compd.* **2019**, *788*, 929–935. [[CrossRef](#)]
12. Chakraborty, S.; Farida, J.J.; Simon, R.; Kasthuri, S.; Mary, N.L. Averrhoë carrambola fruit extract assisted green synthesis of ZnO nanoparticles for the photodegradation of Congo red dye. *Surf. Interfaces* **2020**, *19*, 100488. [[CrossRef](#)]
13. Mallakpour, S.; Behranvand, V. *Nanocomposites Based on Biosafe Nano ZnO and Different Polymeric Matrixes for Antibacterial, Optical, Thermal and Mechanical Applications*; Elsevier Ltd.: Amsterdam, The Netherlands, 2016; Volume 84, ISBN 8415683111.
14. Kadhim, I.H.; Hassan, H.A.; Ibrahim, F.T. Hydrogen gas sensing based on nanocrystalline SnO<sub>2</sub> thin films operating at low temperatures. *Int. J. Hydrogen Energy* **2020**, *45*, 25599–25607. [[CrossRef](#)]
15. Manoj Kumar, P.; Mysamy, K.; Saravanakumar, P.T.; Anandkumar, R.; Pranav, A. Experimental Study on Thermal Properties of Nano-TiO<sub>2</sub> Embedded Paraffin (NEP) for Thermal Energy Storage Applications. *Mater. Today Proc.* **2019**, *22*, 2153–2159. [[CrossRef](#)]
16. Liu, L.; Hu, P.; Li, Y.; An, W.; Lu, J.; Cui, W. P3HT-coated Ag<sub>3</sub>PO<sub>4</sub> core-shell structure for enhanced photocatalysis under visible light irradiation. *Appl. Surf. Sci.* **2019**, *466*, 928–936. [[CrossRef](#)]
17. Borjigin, B.; Ding, L.; Li, H.; Wang, X. A solar light-induced photo-thermal catalytic decontamination of gaseous benzene by using Ag/Ag<sub>3</sub>PO<sub>4</sub>/CeO<sub>2</sub> heterojunction. *Chem. Eng. J.* **2020**, *402*, 126070. [[CrossRef](#)]
18. Sedaghati, N.; Habibi-Yangjeh, A.; Pirhashemi, M.; Asadzadeh-Khaneghah, S.; Ghosh, S. Integration of BiOI and Ag<sub>3</sub>PO<sub>4</sub> nanoparticles onto oxygen vacancy rich-TiO<sub>2</sub> for efficient visible-light photocatalytic decontaminations. *J. Photochem. Photobiol. A Chem.* **2020**, *400*, 112659. [[CrossRef](#)]
19. Boudiaf, S.; Nasrallah, N.; Mellal, M.; Belabed, C.; Belhamdi, B.; Meziani, D.; Mehdi, B.; Trari, M. Synthesis and characterization of semiconductor CoAl<sub>2</sub>O<sub>4</sub> for optical and dielectric studies: Application to photodegradation of organic pollutants under visible light. *Optik* **2020**, *219*, 165038. [[CrossRef](#)]
20. Tab, A.; Bellal, B.; Belabed, C.; Dahmane, M.; Trari, M. Visible light assisted photocatalytic degradation and mineralization of Rhodamine B in aqueous solution by Ag<sub>3</sub>PO<sub>4</sub>. *Optik* **2020**, *214*, 164858. [[CrossRef](#)]
21. Belabed, C.; Bellal, B.; Tab, A.; Dib, K.; Trari, M. Optical and dielectric properties for the determination of gap states of the polymer semiconductor: Application to photodegradation of organic pollutants. *Optik* **2018**, *216*, 218–226. [[CrossRef](#)]
22. Liu, L.; Ding, L.; Liu, Y.; An, W.; Lin, S.; Liang, Y.; Cui, W. A stable Ag<sub>3</sub>PO<sub>4</sub>@PANI core@shell hybrid: Enrichment photocatalytic degradation with π-π conjugation. *Appl. Catal. B Environ.* **2017**, *201*, 92–104. [[CrossRef](#)]
23. Belabed, C.; Rekhila, G.; Douliche, M.; Zitouni, B.; Trari, M. Photo-electrochemical characterization of polypyrrol: Application to visible light induced hydrogen production. *Sol. Energy Mater. Sol. Cells* **2013**, *114*, 199–204. [[CrossRef](#)]
24. Chiu, Y.H.; Chang, T.F.M.; Chen, C.Y.; Sone, M.; Hsu, Y.J. Mechanistic insights into photodegradation of organic dyes using heterostructure photocatalysts. *Catalysts* **2019**, *9*, 430. [[CrossRef](#)]
25. Dias, F.F.; Oliveira, A.A.S.; Arcanjó, A.P.; Moura, F.C.C.; Pacheco, J.G.A. Residue-based iron catalyst for the degradation of textile dye via heterogeneous photo-Fenton. *Appl. Catal. B Environ.* **2016**, *186*, 136–142. [[CrossRef](#)]
26. Cao, Z.; Zhang, T.; Ren, P.; Cao, D.; Lin, Y.; Wang, L.; Zhang, B.; Xiang, X. Doping of chlorine from a neoprene adhesive enhances degradation efficiency of dyes by structured TiO<sub>2</sub>-coated photocatalytic fabrics. *Catalysts* **2020**, *10*, 69. [[CrossRef](#)]

27. Alahiane, S.; Sennaoui, A.; Sakr, F.; Dinne, M.; Qourzal, S.; Assabbane, A. Synchronous role of coupled adsorption-photocatalytic degradation of Direct Red 80 with nanocrystalline TiO<sub>2</sub>-coated non-woven fibres materials in a static batch photoreactor. *Groundw. Sustain. Dev.* **2020**, *11*, 100396. [CrossRef]
28. Ebrahimi, R.; Maleki, A.; Zandsalimi, Y.; Ghanbari, R.; Shahmoradi, B.; Rezaee, R.; Safari, M.; Joo, S.W.; Daraei, H.; Puttaiah, S.H.; et al. Photocatalytic degradation of organic dyes using WO<sub>3</sub>-doped ZnO nanoparticles fixed on a glass surface in aqueous solution. *J. Ind. Eng. Chem.* **2019**, *73*, 297–305. [CrossRef]
29. Kumari, M.; Gupta, S.K. A novel process of adsorption cum enhanced coagulation-flocculation spiked with magnetic nanoadsorbents for the removal of aromatic and hydrophobic fraction of natural organic matter along with turbidity from drinking water. *J. Clean. Prod.* **2020**, *244*, 118899. [CrossRef]
30. Molavi, H.; Shojaei, A.; Pourghaderi, A. Rapid and tunable selective adsorption of dyes using thermally oxidized nanodiamond. *J. Colloid Interface Sci.* **2018**, *524*, 52–64. [CrossRef]
31. Macioszek, V.K.; Kononowicz, A.K. The evaluation of the genotoxicity of two commonly used food colors: Quinoline Yellow (E 104) and Brilliant Black BN (E 151). *Cell. Mol. Biol. Lett.* **2004**, *9*, 107–122. [CrossRef]
32. Lau, K.; McLean, W.G.; Williams, D.P.; Howard, C.V. Synergistic interactions between commonly used food additives in a developmental neurotoxicity test. *Toxicol. Sci.* **2006**, *90*, 178–187. [CrossRef]
33. Belabed, C.; Abdi, A.; Benabdelghani, Z.; Rekhila, G.; Etxeberria, A.; Trari, M. Photoelectrochemical properties of doped polyaniline: Application to hydrogen photoproduction. *Int. J. Hydrogen Energy* **2013**, *38*, 6593–6599. [CrossRef]
34. Regulska, E.; Brus, D.M.; Rodziewicz, P.; Sawicka, S.; Karpinska, J. Photocatalytic degradation of hazardous Food Yellow 13 in TiO<sub>2</sub> and ZnO aqueous and river water suspensions. *Catal. Today* **2016**, *266*, 72–81. [CrossRef]
35. Gupta, V.K.; Jain, R.; Agarwal, S.; Nayak, A.; Shrivastava, M. Photodegradation of hazardous dye quinoline yellow catalyzed by TiO<sub>2</sub>. *J. Colloid Interface Sci.* **2012**, *366*, 135–140. [CrossRef] [PubMed]
36. Salem, M.A.; Al-Ghonemiy, A.F.; Zaki, A.B. Photocatalytic degradation of Allura red and Quinoline yellow with Polyaniline/TiO<sub>2</sub> nanocomposite. *Appl. Catal. B Environ.* **2009**, *91*, 59–66. [CrossRef]
37. Shen, Y.; Zhu, Z.; Wang, X.; Khan, A.; Gong, J.; Zhang, Y. Synthesis of Z-scheme g-C<sub>3</sub>N<sub>4</sub>/Ag/Ag<sub>3</sub>PO<sub>4</sub> composite for enhanced photocatalytic degradation of phenol and selective oxidation of gaseous isopropanol. *Mater. Res. Bull.* **2018**, *107*, 407–415. [CrossRef]
38. Du, J.; Ma, S.; Yan, Y.; Li, K.; Zhao, F.; Zhou, J. Corn-silk-templated synthesis of TiO<sub>2</sub> nanotube arrays with Ag<sub>3</sub>PO<sub>4</sub> nanoparticles for efficient oxidation of organic pollutants and pathogenic bacteria under solar light. *Colloids Surf. A Physicochem. Eng. Asp.* **2019**, *572*, 237–249. [CrossRef]
39. Luo, L.; Li, Y.; Hou, J.; Yang, Y. Visible photocatalysis and photostability of Ag<sub>3</sub>PO<sub>4</sub> photocatalyst. *Appl. Surf. Sci.* **2014**, *319*, 332–338. [CrossRef]
40. Gaya, U.I.; Abdullah, A.H. Heterogeneous photocatalytic degradation of organic contaminants over titanium dioxide: A review of fundamentals, progress and problems. *J. Photochem. Photobiol. C Photochem. Rev.* **2008**, *9*, 1–12. [CrossRef]
41. Zhang, H.; Huang, H.; Ming, H.; Li, H.; Zhang, L.; Liu, Y.; Kang, Z. Carbon quantum dots/Ag<sub>3</sub>PO<sub>4</sub> complex photocatalysts with enhanced photocatalytic activity and stability under visible light. *J. Mater. Chem.* **2012**, *22*, 10501–10506. [CrossRef]

**Publisher's Note:** MDPI stays neutral with regard to jurisdictional claims in published maps and institutional affiliations.



© 2020 by the authors. Licensee MDPI, Basel, Switzerland. This article is an open access article distributed under the terms and conditions of the Creative Commons Attribution (CC BY) license (<http://creativecommons.org/licenses/by/4.0/>).